Electronic Supplementary Information

Reduced graphene oxide–silicon interface involving direct Si–O covalent bonding as a conductive and mechanical stable ohmic contact

Soraya Rahpeima,[ab] Essam M. Dief,[a] Chandramalika R.Peiris,[a] Stuart Ferrie,[a] Alex Duan,[c] Simone Ciampi,[a] Colin L. Raston*[b] and Nadim Darwish*[a]

[a] School of Molecular and Life Sciences, Curtin Institute of Functional Molecules and Interfaces, Curtin University, Bentley, WA 6102, Australia
[b] Flinders Institute for Nanoscale Science and Technology, College of Science and Engineering, Flinders University, Adelaide, SA 5001, Australia
[c] Trace Analysis for Chemical, Earth and Environmental Sciences (TrACEES), The University of Melbourne, Melbourne, VIC 3010, Australia

Emails: nadim.darwish@curtin.edu.au; colin.raston@flinders.edu.au
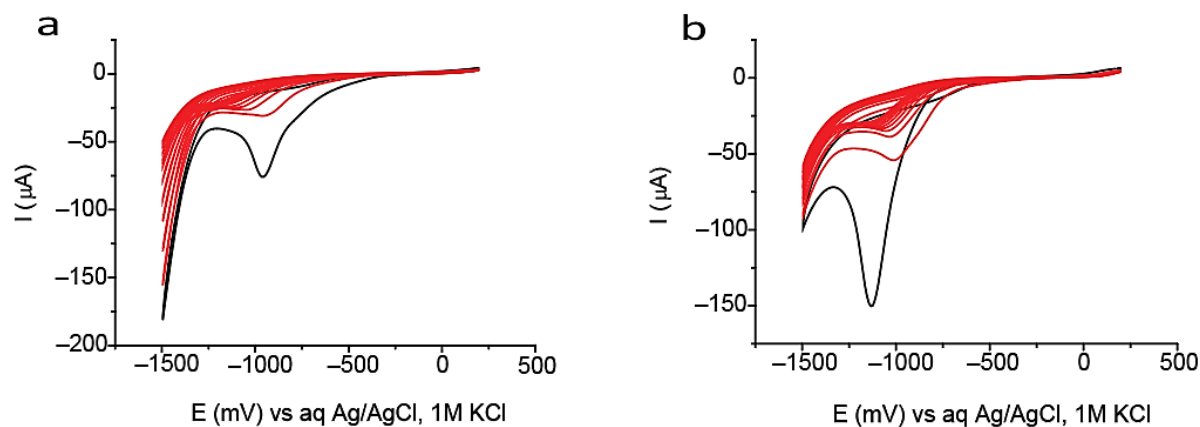
Fig. S1. Electrochemical reduction of GO in 0.1 M phosphate buffer solution at pH 7.4 at a scan rate of (a) 25 mV/s and (b) 100 mV/s. The potential is presented in mV versus aq Ag/AgCl, 1 M KCl, ranging from −1500 mV to +200 mV.
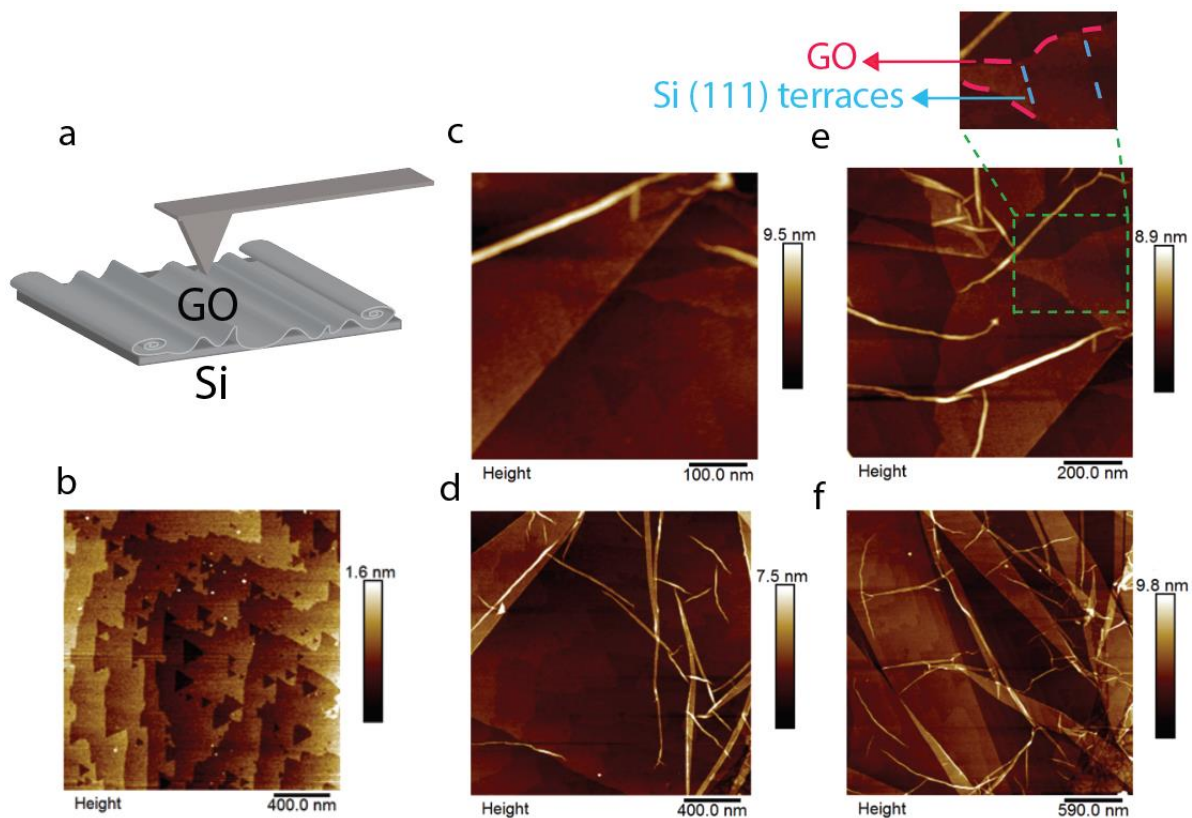
Fig. S2. Schematic describing the AFM experiment of the Si–GO surface (a). Topography image of unmodified Si (111)–H surface (b). Topography images of representative Si–GO surfaces (c-f). Inset in (e) shows a monolayer of GO covering Si (111) terraces. The GO monolayer follows the topography of the Si (111) terraces – preventing Si from oxidation.
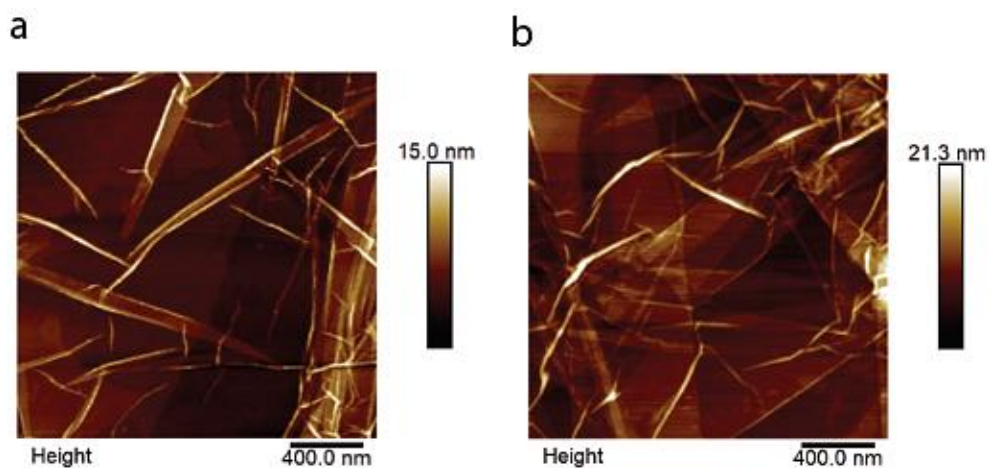

Fig. S3. Topography images of representative areas of the Si–GO surfaces that showed the presence of significant amount of wrinkles (a,b).

2
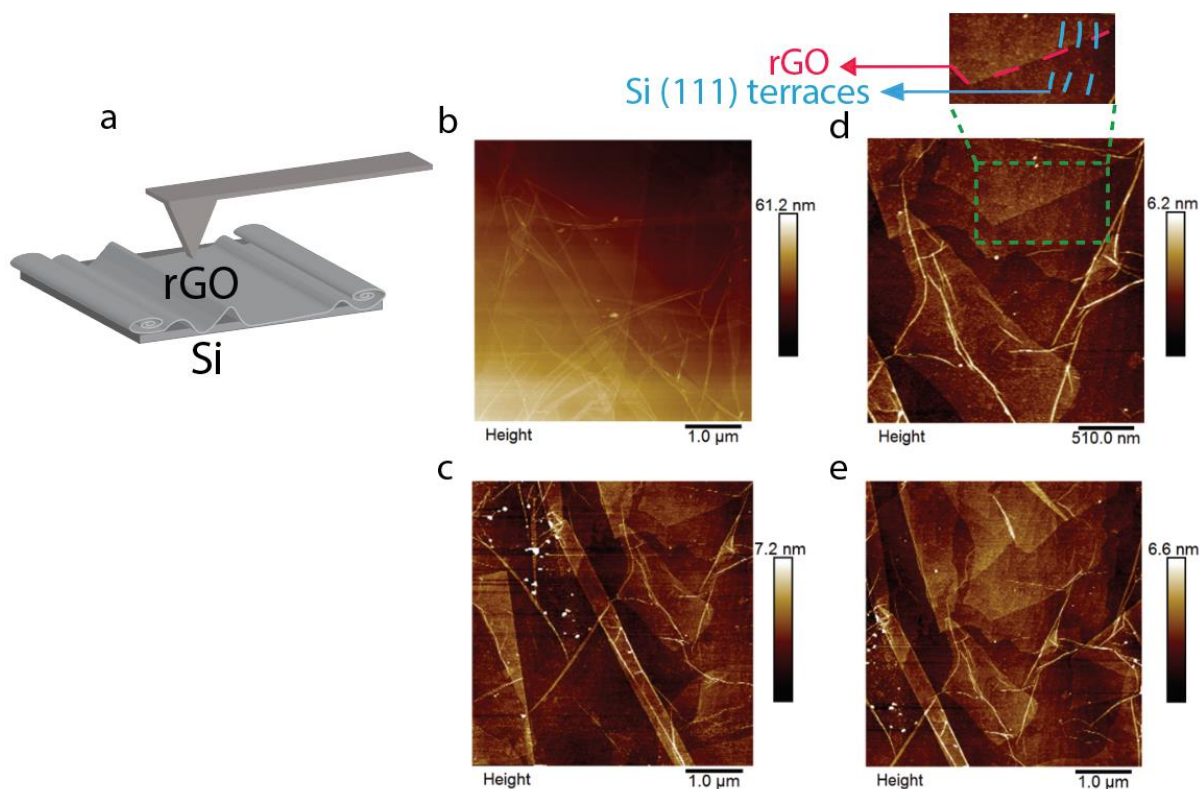
Fig. S4. Schematic describing the AFM experiment of the Si–rGO surface, i.e. Si–GO, after electrochemical reduction (a). Topography images of representative Si–rGO surfaces (b-f). Inset in (d) shows a monolayer of rGO covering Si (111) terraces. The electrochemical transformation of GO into rGO occurs without desorption of the layers from the Si surface.
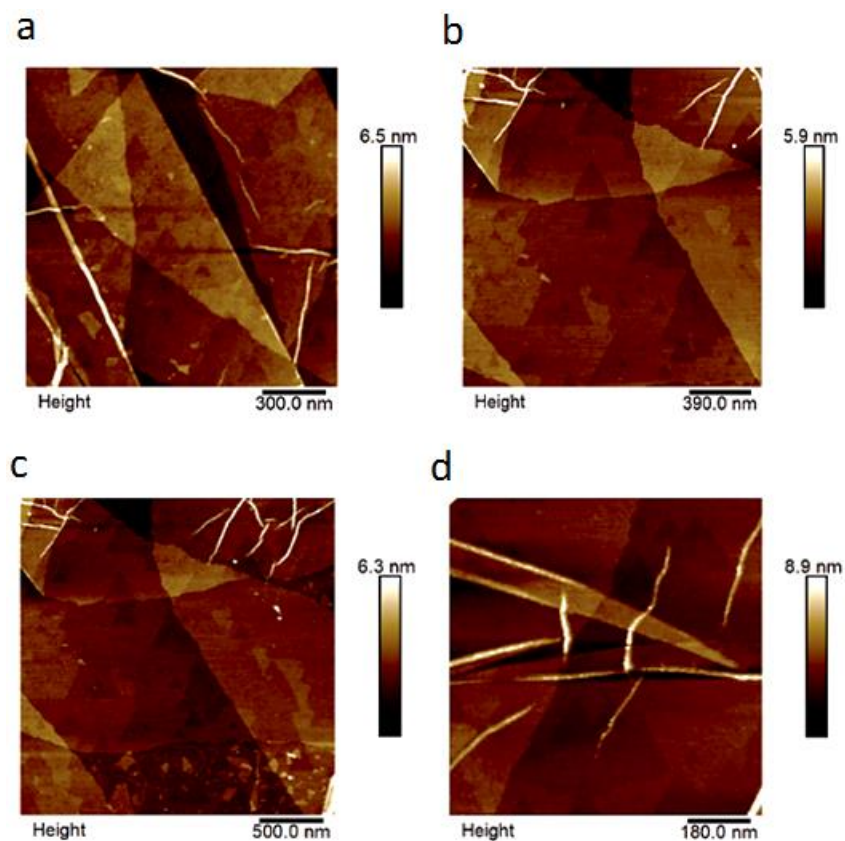
Fig. S5. Topography images of representative Si–GO surfaces (a–d). Silicon terraces are visible underneath the GO layers with limited protrusions (white spots) indicating limited oxidation of the Si.
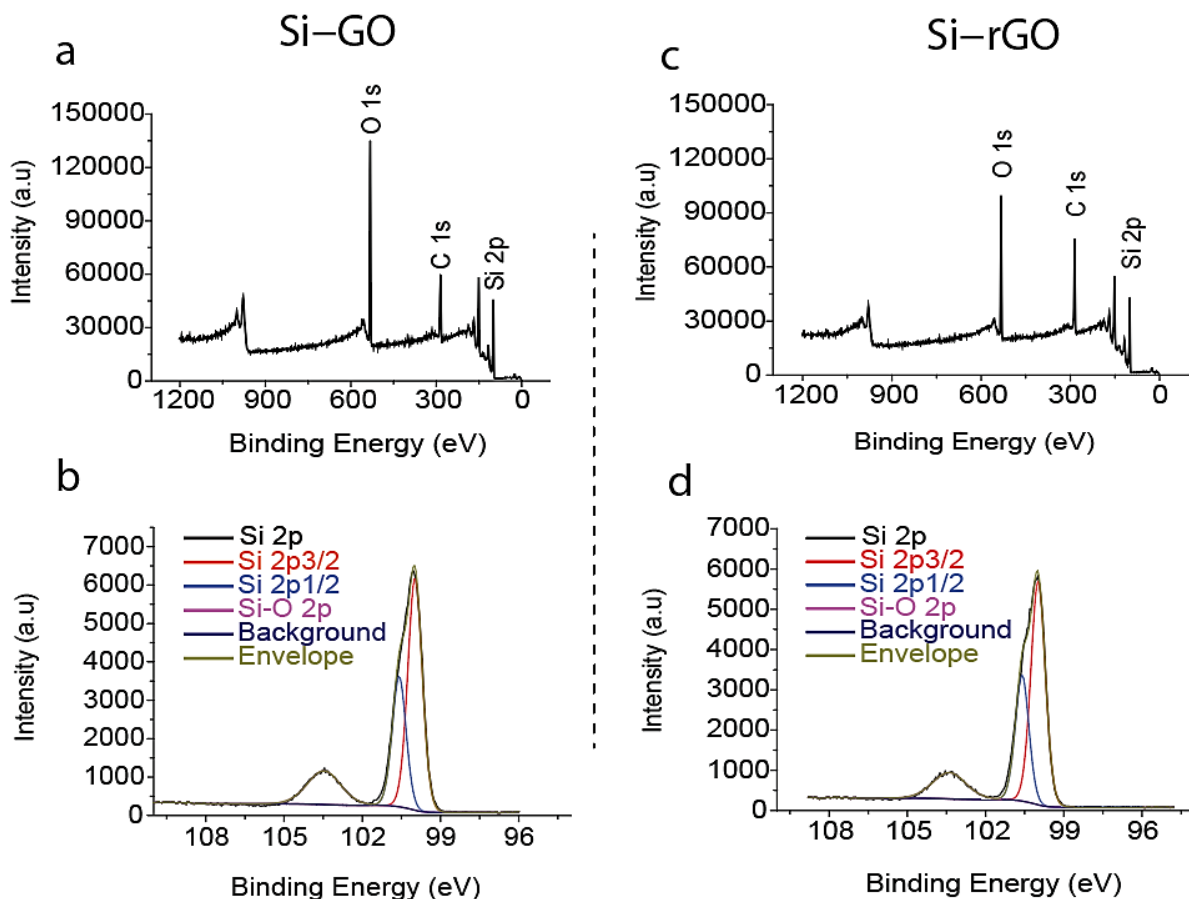
**Fig S6.** Survey and silicon high resolution scans of Si–GO (a, b) and of Si–rGO (c, d). The presence of peaks in the 102–104 eV range is assigned to the Si–O–C of the Si–GO and Si–rGO, respectively. The assignment of a Si–O–C is supported by (a) limited change in the signal before and after electrochemical reduction, obviating the possibility of SiOx which would otherwise significantly increase after extensive cyclic voltammetry, and (b) the XPS signal is significantly large, noting that if the signal is due to SiOx, the oxide should be clearly visible in AFM images. Moreover, AFM images clearly show Si (111) terraces underneath the GO and the rGO layers – an observation that is not possible if SiOx is present on the surface.
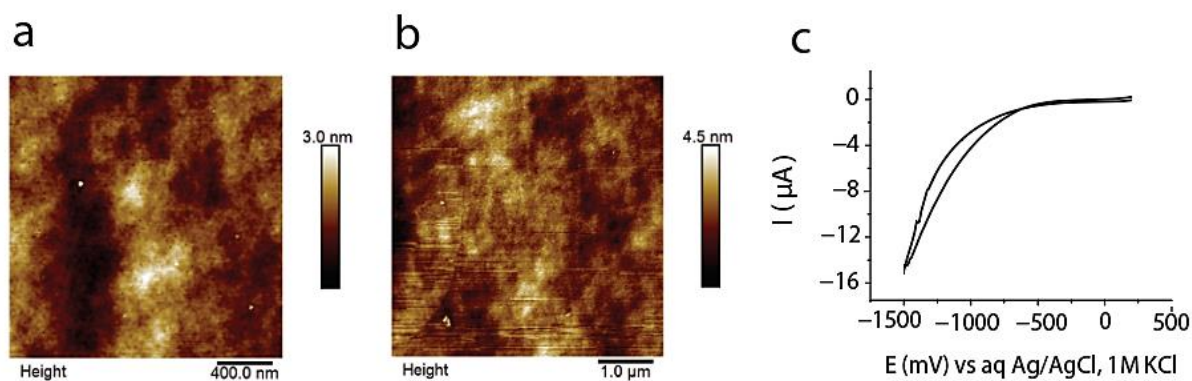

Fig. S7. Topography images of representative Si–Ox surfaces incubated in GO for 24 h (a,b), and electrochemical reduction of the corresponding surfaces in 0.1 M phosphate buffer solution at pH 7.4 and a scan rate of 50 mV/s. The potential in (c) is presented in mV versus aq Ag/AgCl, 1 M KCl.
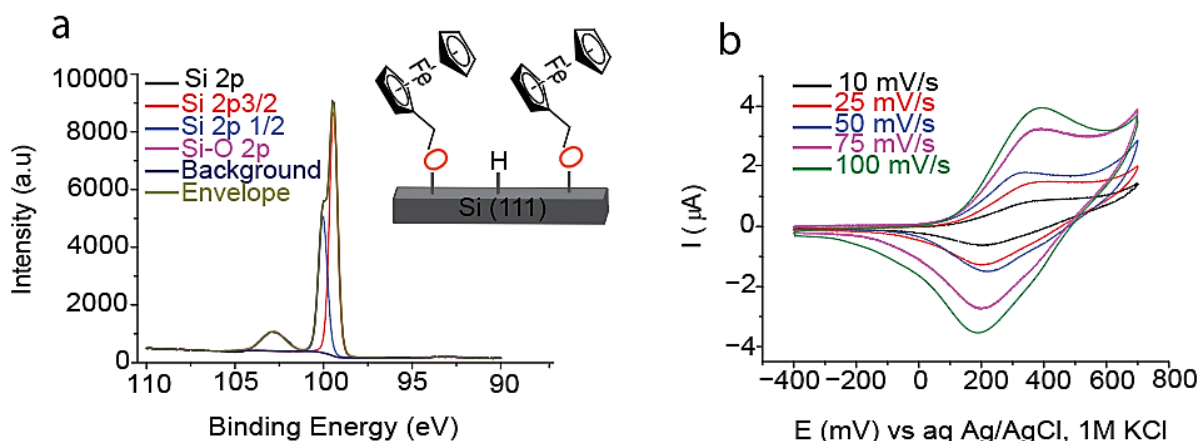
Fig S8. XPS Si high resolution scans of ferrocene methanol monolayer formed on Si (111)–H surface (a), cyclic voltammetry curves for ferrocene methanol on Si (111)–H at different scan rates (b). The presence of Si–O bonding in XPS and surface-bound ferrocene signals in cyclic voltammetry indicated the formation of Si–O–C bonded monolayer.
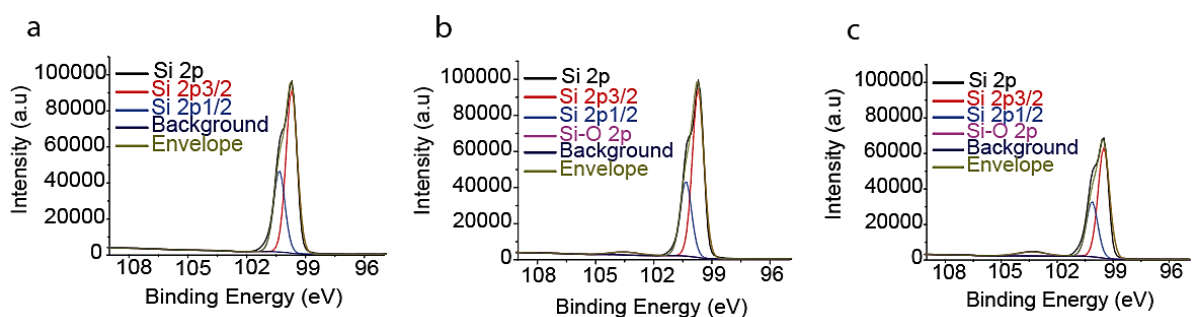

Fig S9. XPS Si high resolution scans of freshly prepared Si–H surface (a), after 24 h incubation in water (b) and after 48 h incubation in water (c). The presence of peaks in the 102–104 eV range is assigned to the Si–Ox and the integrated peak is 0% in (a), 3% in (b) and 7% in (c) relative to the Si 2p.
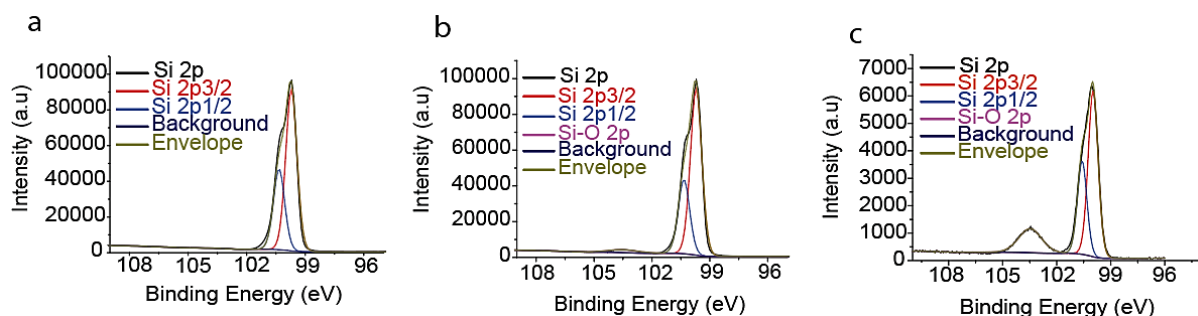
Fig. S10. XPS high resolution scans of freshly prepared Si–H surface (a), after 24 h incubation in water (b), and after incubation in 2 mg/ml GO suspension in water forming the Si–GO interface (c). The presence of weak emission in the 102–104 eV range in (b) is assigned to Si-Ox while that in (c) is assigned to the Si–O–C upon the reaction of Si–H with GO. The integrated peak area of the SiOx emission at 103 eV with respect to the Si 2p emission is 0%, 3% and 21% for (a), (b) and (c), respectively suggesting that the strong emission in (c) is largely due to the covalent attachment of GO with Si–H via Si–O–C bond.
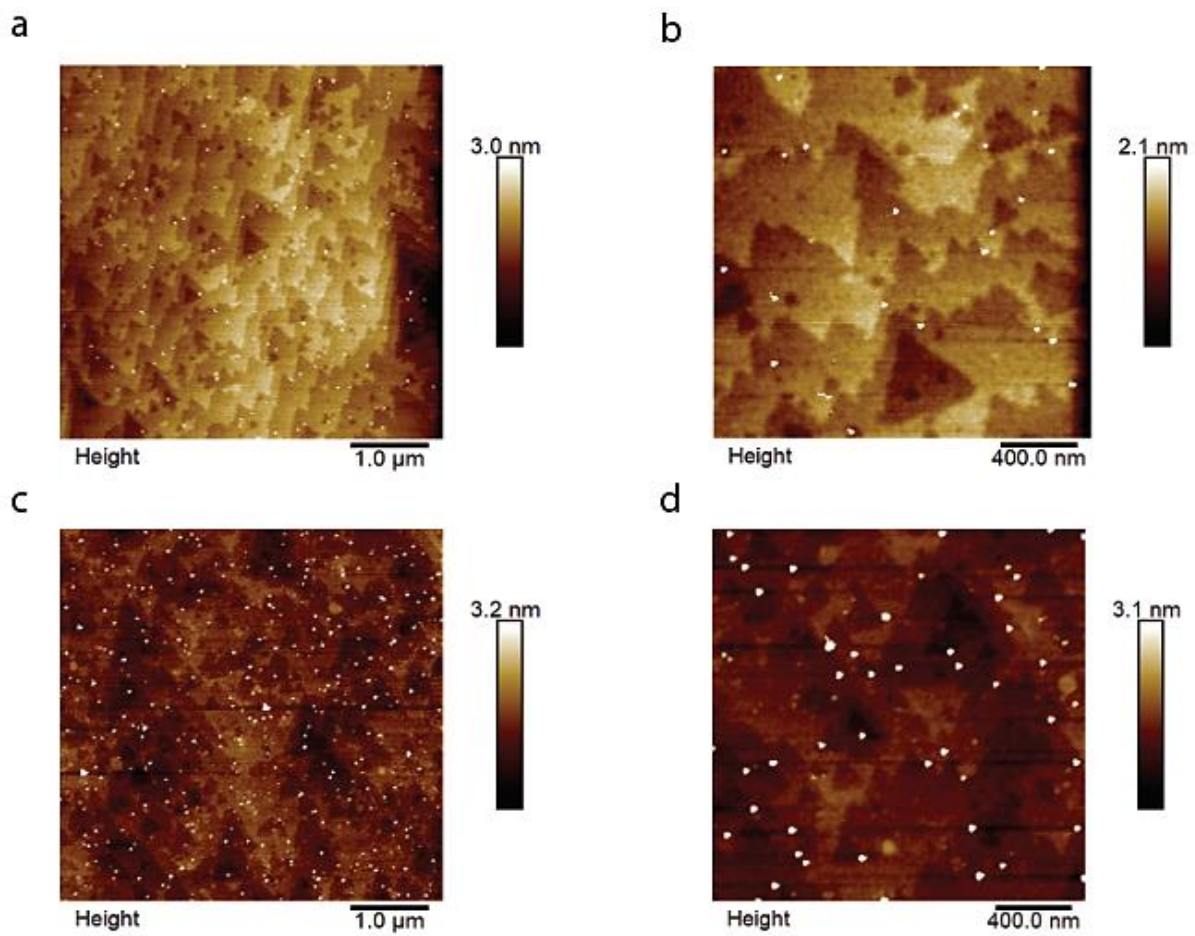
Fig. S11. Topography images of representative freshly prepared Si–H surface after 48 h (a,b) and 72 h (c,d) incubation in water.
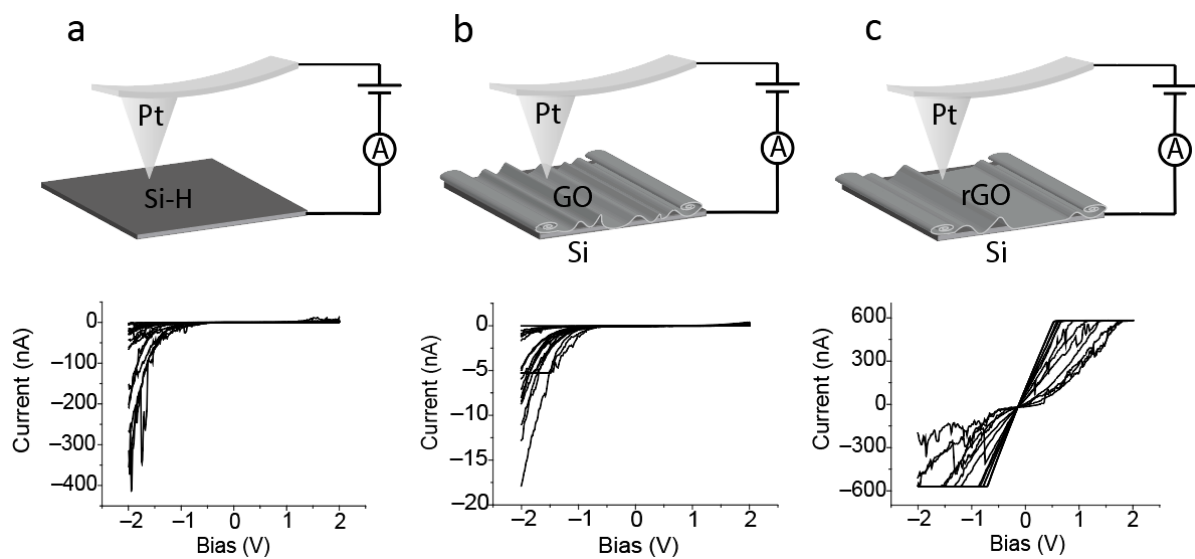
Fig S12. An overlay of current–voltage measurements for (a) Si–H–Pt junction, (b) Si–GO–Pt junction, and (c) Si–rGO–Pt junction. The bias is applied to the silicon surface. The rectifying junction in (a) and (b) changes to ohmic after electrochemical reduction of GO in (c). Current saturation is reached beyond a voltage of ±0.6 V.
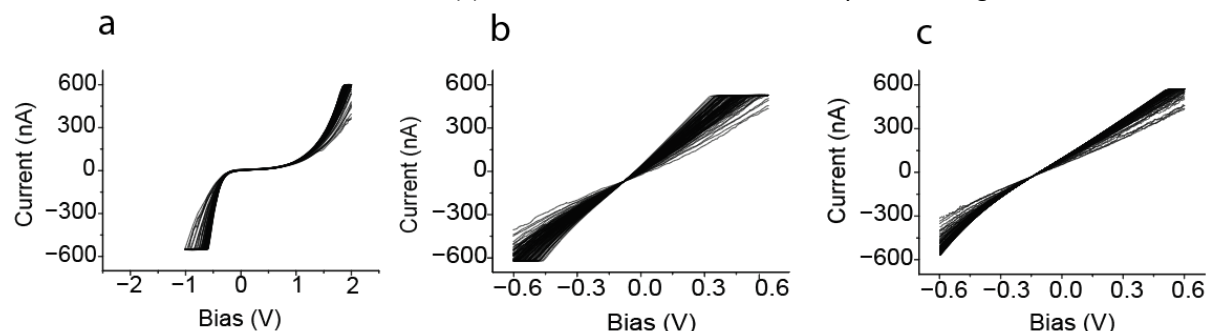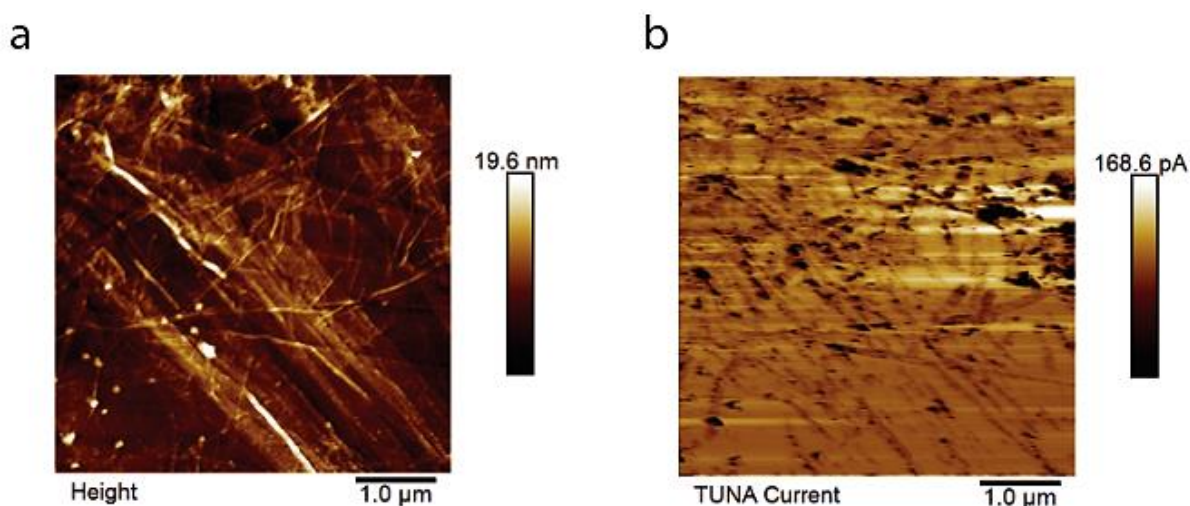

Fig. S13. An overlay of 100 different current–voltage measurements of Si–rGO–Pt junction for 1 reduction cycle (a), 5 reduction cycles (b), and 10 reduction cycles (c). The bias is applied to the silicon surface. Current saturation is reached beyond a voltage of ±0.6 V in (b) and (c).

Fig. S14. Topography image (a) and current mapping (b) of representative Si–rGO surfaces (obtained after electrochemical reduction of Si–GO for 10 cycles). The current images were obtained using the peak force tunnelling AFM mode with peak force set-point to 50nN and a bias voltage of + 2 V applied to the Si surface. The I–V curves were taken at voltage sweep rates of 1 V/s and with the feedback being switched to contact mode with the deflection set-point kept constant to 500 nN. The deflection set-point corresponding to 500 nN was chosen such that the current through the contact becomes independent on the force.

Experimental section

All chemicals used are of analytical grade. Graphene oxide (GO) (Sigma-Aldrich, dispersion in H_2O with concentration of 2 mg/mL) was used as received. Hydrogen peroxide (30 wt % in water) and sulfuric acid (PuranalTM, 95–97%), ammonium fluoride (PuranalTM, 40 wt % in water) and ammonium sulfite monohydrate ((NH_4)$_2SO_3$, 92%) were purchased from Sigma-Aldrich and used for Si wafer cleaning and etching, respectively. Dichloromethane (DCM), isopropanol and Mili-Q-water (>18 MΩ cm) were utilized for pre-Si surface cleaning. N–type (phosphorus doped) single-side-polished Si wafers were purchased from Siltronix, S.A.S. (Archamps, France) with 500–550 µm of thickness and (111) ± 0.05°

7

(with resistivity of 0.003–0.007 Ω cm). Sodium dihydrogen orthophosphate ($NaH_2PO_4.2H_2O$) and di-sodium hydrogen orthophosphate, dodecahydrate ($Na_2HPO_4.12H_2O$) were purchased from Ajax Finechem as supporting electrolyte for the electrochemical reduction procedure of GO.

The Si cleaning and etching procedure were carried out based on recent literature. [1-3] Briefly, DCM, Isopropanol and Milli-Q water were used for washing Si wafers which were then cleaned using piranah solution (3 H_2SO_4: 1 H_2O_2 (V/V)) at 130 °C for 30 min. The surfaces were subsequently etched in deoxygenated 40 wt % aqueous ammonium fluoride solution in the presence of small amount of ammonium sulfite monohydrate (~5 mg) for 13 min to remove native oxygen layer on the Si surface and obtain Si-hydride (Si–H). The etched surface was rinsed using Milli-Q water and DCM, dried by nitrogen gas, and directly immersed in an aqueous suspension of GO (which was pre-treated by ultrasonication for 30 min) for 24 h to make robust attachment.

The electrochemical experiments were carried out using CH Instrument, USA (CHI650) and a conventional three-electrode cell, with an Ag/AgCl aqueous electrode, 1 M KCl and platinum wire as reference and counter electrodes, respectively. The electrochemical reduction of GO was performed directly after the attachment of GO on the Si–H surface. The electrochemical reduction was carried out at different scan rates (25, 50, 100, 200 and 500 mV/s) and in a potential window ranging from −1500 to +200 mV versus Ag/AgCl, 1 M KCl. All experiments have been carried out in a of 0.1 M phosphate buffer solution (pH 7.4).

XPS data was acquired using a Kratos Axis ULTRA X-ray Photoelectron Spectrometer incorporating a 165mm hemispherical electron energy analyser. The incident radiation was Monochromatic Al Kα X-rays (1486.6 eV) at 150W (15kV, 15 ma). Survey (wide) scans were taken at an analyser pass energy of 160eV and multiplex (narrow) high resolution scans at 20 eV. Scanned area is about 0.8 mm x 0.3 mm and the depth is less than 10nm (volume is approx. 2400 cubic micron). The experiment was conducted under a base pressure in the analysis chamber approx. 1.0×10^{-9} torr and during sample analysis 1.0×10^{-8} torr. Survey scans were carried out over 1200-0eV binding energy range with 1.0 eV steps and a dwell time of 100 ms. Narrow high-resolution scans were run with 0.05 eV steps and 250 ms dwell time. Data analysis and curve fitting was performed using CasaXPS software and the binding energies of C 1s in survey scan and C–C bond in high resolution scan were calibrated to be 285.0 eV.

Atomic Force Microscopy

All atomic force microscopy images were obtained using a Bruker Dimension AFM microscopy. The topography images were obtained in tapping mode in air at room temperature using silicon nitride cantilevers (TESPA-V2 from Bruker). Sample topographies and dc conductivities were imaged with a Bruker Dimension Icon atomic force microscope. Data were obtained in air at room temperature and using conductive platinum tips (Rocky Mountain Nanotechnology AFM probes, 25Pt300B, with spring constant of 18 N m^{-1}). The imaging resolution was set to 256 points/line, the scan rate to 1 Hz and the peak force setpoint to 50 nN. The I–V curves were taken at voltage sweep rates of 1 V/s and with the feedback being switched to contact mode with the deflection set-point kept constant to 500 nN. The deflection setpoint corresponding to 500 nN was chosen such that the current through the contact becomes independent on the force.

References

1.   A. C. Aragonès, N. Darwish, S. Ciampi, F. Sanz, J. J. Gooding and I. Díez-Pérez, *Nat. Commun.*, 2017, 8, 1-8.
2.   C. R. Peiris, Y. B. Vogel, A. P. Le Brun, A. C. Aragonès, M. L. Coote, I. Díez-Pérez, S. Ciampi and N. Darwish, *J. Am. Chem. Soc.*, 2019, 141, 14788-14797.
3.   L. Zhang, E. Laborda, N. Darwish, B. B. Noble, J. H. Tyrell, S. Pluczyk, A. P. Le Brun, G. G. Wallace, J. Gonzalez and M. L. Coote, *J. Am. Chem. Soc.*, 2018, 140, 766-774.